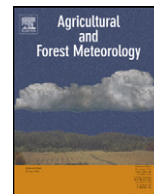




Contents lists available at SciVerse ScienceDirect

Agricultural and Forest Meteorology

journal homepage: www.elsevier.com/locate/agrformet

Estimating leaf carotenoid content in vineyards using high resolution hyperspectral imagery acquired from an unmanned aerial vehicle (UAV)

P.J. Zarco-Tejada^{a,*}, M.L. Guillén-Climent^a, R. Hernández-Clemente^b, A. Catalina^c,
M.R. González^c, P. Martín^c

^a Instituto de Agricultura Sostenible (IAS), Consejo Superior de Investigaciones Científicas (CSIC), Córdoba, Spain

^b ETSIAM, Departamento de Ingeniería Forestal, Universidad de Córdoba, Córdoba, Spain

^c Departamento de Producción Vegetal y Recursos Forestales, ETS de Ingenierías Agrarias, Universidad de Valladolid, Palencia, Spain

ARTICLE INFO

Article history:

Received 14 February 2012

Received in revised form

29 September 2012

Accepted 30 December 2012

Keywords:

Hyperspectral

Airborne

Carotenoid

Chlorophyll

 R_{515}/R_{570}

UAV

ABSTRACT

Chlorophyll *a+b* (C_{a+b}) and carotenoids (C_{x+c}) are leaf pigments associated with photosynthesis, participation in light harvesting and energy transfer, quenching and photoprotection. This manuscript makes progress on developing methods for leaf carotenoid content estimation, using high resolution hyperspectral imagery acquired from an unmanned aerial vehicle (UAV). Imagery was acquired over 3 years using two different UAV platforms, a 6-band multispectral camera and a micro-hyperspectral imager flown with 260 bands at 1.85 nm/pixel and 12-bit radiometric resolution, yielding 40 cm pixel size and a FWHM of 6.4 nm with a 25- μ m slit in the 400–885 nm spectral region. Field data collections were conducted in August 2009–2011 in the western area of Ribera del Duero *Appellation d'Origine*, northern Spain. A total of twelve full production vineyards and two study plots per field were selected to ensure appropriate variability in leaf biochemistry and vine physiological conditions. Leaves were collected for destructive sampling and biochemical determination of chlorophyll *a+b* and carotenoids conducted in the laboratory. In addition to leaf sampling and biochemical determination, canopy structural parameters, such as grid size, number of vines within each plot, trunk height, plant height and width, and row orientation, were measured on each 10 m \times 10 m plot. The R_{515}/R_{570} index recently proposed for carotenoid estimation in conifer forest canopies was explored for vineyards in this study. The PROSPECT-5 leaf radiative transfer model, which simulates the carotenoid and chlorophyll content effects on leaf reflectance and transmittance, was linked to the SAILH and FLIGHT canopy-level radiative transfer models, as well as to simpler approximations based on infinite reflectance R_{∞} formulations. The objective was to simulate the pure vine reflectance without soil and shadow effects due to the high resolution hyperspectral imagery acquired from the UAV, which enabled targeting pure vines. The simulation results obtained with synthetic spectra demonstrated the effects due to C_{a+b} content on leaf C_{x+c} estimation when the R_{515}/R_{570} index was used. Therefore, *scaling up* methods were proposed for leaf carotenoid content estimation based on the combined R_{515}/R_{570} (sensitive to C_{x+c}) and TCARI/OSAVI (sensitive to C_{a+b}) narrow-band indices. Results demonstrated the feasibility of mapping leaf carotenoid concentration at the pure-vine level from high resolution hyperspectral imagery, yielding a root mean square error (RMSE) below 1.3 μ g/cm² and a relative RMSE (R-RMSE) of 14.4% (FLIGHT) and 12.9% (SAILH) for the 2 years of hyperspectral imagery. The simpler formulation based on the infinite reflectance model by Yamada and Fujimura yielded lower errors (RMSE = 0.87 μ g/cm²; R-RMSE < 9.7%), although the slope deviated more from the 1:1 line. Maps showing the spatial variability of leaf carotenoid content were estimated using this methodology, which targeted pure vines without shadow and background effects.

© 2013 Elsevier B.V. All rights reserved.

1. Introduction

Leaf biochemical constituents, such as chlorophyll *a+b* (C_{a+b}), water (C_w) and dry matter (C_m), are physiological indicators used as a proxy of stress that can be estimated by remote sensing data in the 400–2500 nm spectral region. In particular, several studies demonstrate that estimating chlorophyll content in leaves is feasible using leaf reflectance and transmittance (Jacquemoud et al., 1996; Carter

* Corresponding author at: Instituto de Agricultura Sostenible (IAS), Consejo Superior de Investigaciones Científicas (CSIC), Alameda del Obispo, s/n, 14004 Córdoba, Spain. Tel.: +34 957 499 280/676 954 937; fax: +34 957 499 252.

E-mail addresses: pzarco@ias.csic.es, pablo.zarco@csic.es (P.J. Zarco-Tejada).

and Spiering, 2002; Sims and Gamon, 2002; Gitelson et al., 2003; le Maire et al., 2004). For this purpose, a large number of narrow-band indices calculated from hyperspectral reflectance have been proposed with success in different crops (Haboudane et al., 2002, 2004; Zarco-Tejada et al., 2001; a full review of indices can be found in Zarco-Tejada et al., 2005). Recently, combined indices sensitive to C_{a+b} content have been developed with the Transformed Chlorophyll Absorption in Reflectance Index, TCARI (Haboudane et al., 2002), and the Optimized Soil-adjusted Vegetation Index, OSAVI (Rondeaux et al., 1996), used to minimize soil and leaf area index (LAI) effects in closed crops (Haboudane et al., 2002), tree orchards (Zarco-Tejada et al., 2004) and vineyards (Zarco-Tejada et al., 2005; Martin et al., 2007; Meggio et al., 2010).

Carotenoids (C_{x+c}), which include two carotenes and five xanthophylls, are also important photosynthetic pigments (Demmig-Adams and Adams, 1992). Carotenoids are physiologically relevant because of their role associated with photosynthesis, participation in light harvesting and energy transfer (Frank and Cogdell, 1996; Ritz et al., 2000), quenching and photoprotection (Thayer and Björkman, 1990; Young and Britton, 1990; Demmig-Adams, 1998). Nevertheless, less research has been conducted on carotenoid content estimation due to the difficulties associated with the overlapping absorption in the blue/green region by photosynthetic pigments such as C_{a+b} , C_{x+c} and anthocyanins (Anth). The overlapping absorption by chlorophyll and carotenoids in the 400–700 nm region poses a problem when trying to retrieve both C_{a+b} and C_{x+c} concentration independently (Feret et al., 2011). In addition, some indices have been identified as sensitive to C_{x+c} ; they generally work well at the leaf level but there are considerable effects caused by canopy structure and background when they are applied to reflectance imagery (Meggio et al., 2010; Hernández-Clemente et al., 2011). Furthermore, achieving progress on carotenoid content estimation has become even more difficult in vineyards because they are complex heterogeneous canopies, with large effects caused by shadows and soil components as a function of sun angle and row orientation.

The main spectral bands proposed for C_{x+c} estimation in the visible/NIR region are based on band ratios in the 700 nm region (678, 708 and 760 nm) and the green region (500 and 550 nm) (Chappelle et al., 1992; Merzlyak et al., 1999). In addition, some indices have been proposed using the 800 nm band combined with 470, 680, and 635 nm bands (Peñuelas et al., 1995; Blackburn, 1998). In particular, the work conducted by Chappelle et al. (1992) concluded that C_{x+c} showed a maximum absorption peak at 500 nm, proposing ratios such as R_{760}/R_{500} for C_{x+c} estimation. Other authors (Gamon et al., 1992; Gitelson et al., 2003; Garrity et al., 2011; Hernández-Clemente et al., 2011) proposed visible ratios. Specific leaf-level studies conducted by Gitelson et al. (2002) showed that C_{x+c} effects on the leaf reflectance were directly related to a spectral absorption at 520 nm. They proposed the Carotenoid Concentration Index (CCI) as $(1/R_{515}) - (1/R_{550})$ and $(1/R_{515}) - (1/R_{700})$ (Gitelson et al., 2002). The CCI formulation was developed because reflectance at 515 nm was highly sensitive to carotenoid content at the leaf level but was also found to be affected by chlorophyll content. The authors subtracted the chlorophyll content effect using the reciprocal reflectance at 550 nm or at 700 nm. Although these formulations showed good correlations at the leaf level, they were highly affected by the structure when applied to canopy level data (Hernández-Clemente et al., 2012).

However, these studies relied entirely on leaf-level work and required *scaling up* to the canopy level, assessing the effects on the proposed indices caused by structure and background due to mixed pixels. In particular, the validity of leaf-level indices for pigment content estimation in vineyards from airborne imagery was studied through the linked PROSPECT (Jacquemoud and Baret, 1990) and rowMCRM models. Through this approach, the effects of vineyard

structure, vine dimensions, row orientation, and soil and shadow effects on canopy reflectance could be assessed for C_{a+b} estimation (Zarco-Tejada et al., 2005). Using this methodology, relationships for C_{a+b} content with TCARI/OSAVI enabled mapping chlorophyll in 24 vineyards using CASI airborne imagery, yielding $r^2 = 0.67$ and a root mean square error (RMSE) of $11.5 \mu\text{g}/\text{cm}^2$.

These methods that require accounting for row structure and orientation, soil effects and canopy LAI variation may be critical for vineyards when using image resolutions in the range of 1–2 m pixel size. The pure vine reflectance cannot be extracted without soil and shadow contributions at spatial resolutions greater than 1 m. Nevertheless, simpler canopy-level approximations with no structure considerations may work well when higher spatial resolution is used (below 50 cm pixel size for vineyards) because the extraction of the pure vine reflectance by reducing shadow and soil background contributions is then feasible. Under these assumptions of targeting pure dense vines, infinite reflectance formulations may be proposed as a simpler approximation since they model the reflectance without canopy structure or viewing geometry considerations and are based solely on leaf reflectance and transmittance (see Zarco-Tejada et al., 2001 for a review of infinite reflectance models). These formulations are valid for optically thick leaf material, with different assumptions for the multiple scattering. Lillestaeter (1982), Miller et al. (1992), Yamada and Fujimura (1991) and Hapke (1993) discussed these infinite reflectance models, applied with success to forest sites for C_{a+b} estimation (Zarco-Tejada et al., 2001) and for equivalent water thickness estimation (Riaño et al., 2005).

More complex approaches can also be applied to model the pure vine reflectance when using high resolution that enables the removal of mixed pixels and shadow effects. Under these conditions, approximations based on turbid-medium assumptions, such as with SAILH when targeting pure canopy pixels (Zarco-Tejada et al., 2001) and more computationally expensive approximations such as in the Forest Light Interaction Model (FLIGHT) may be more appropriate. In particular, the 3D FLIGHT model is based on the Monte Carlo ray tracing method to simulate radiative transfer in a canopy structure (North, 1996), and was previously used to simulate row-structured canopy reflectance in olive orchards (Suárez et al., 2008) and, more recently, to simulate row-structured peach and orange orchards for fPAR estimation (Guillén-Climent et al., 2012).

Therefore, the assessment of a leaf C_{x+c} sensitive index linked to different *scaling up* approaches is the main focus of this manuscript. Recently, the R_{515}/R_{570} index was proposed by Hernández-Clemente et al. (2012) for forestry sites, demonstrating to be significantly related to leaf C_{x+c} concentration both at leaf ($r^2 > 0.72$; $P < 0.001$) and canopy ($r^2 > 0.71$; $P < 0.001$) levels. In that study, coefficients of determination between leaf C_{x+c} concentration and other published narrow-band indices sensitive to C_{x+c} revealed that such indices were highly related to C_{x+c} content at leaf level but highly affected by structural parameters at crown level. Nevertheless, the effects of C_{a+b} content on this proposed R_{515}/R_{570} index have not been assessed yet. This manuscript proposes the estimation of both C_{x+c} and C_{a+b} at the leaf level using R_{515}/R_{570} and TCARI/OSAVI indices simultaneously through a *scaling up* approach based on different canopy reflectance simulations.

2. Materials and methods

2.1. Field experiments and airborne campaigns

2.1.1. Field data collection

Field data collections were conducted in August 2009–2011 in the western area of Ribera del Duero *Appellation d'Origine*

(northern Spain). A total of 12 full production vineyards were selected to ensure appropriate variability in leaf biochemistry and vine physiological conditions. All vineyards consisted of cv. Tempranillo grafted on 110-Richter rootstock, with ages ranging between 7 and 16 years. The soils were calcareous and poor in organic matter, with a medium-weighted texture and an average pH of 8.7. Concentrations of active carbonate (up to 17.6%) and DPTA extractable Fe ($1.2\text{--}7.6\text{ mg kg}^{-1}$) were highly heterogeneous within the study areas. The field data collection was conducted in 24 sub-areas of $10\text{ m} \times 10\text{ m}$ (2 sub-areas in each selected vineyard). Plant density was 2200 vines per hectare, and plants were trained to a simple or double Cordon Royat system (as described in detail in Martin et al., 2007). The vineyards under study ranged in physiological status, canopy structure, soil background, and planting row orientation.

The leaves used for destructive sampling and biochemical determination were sampled from the top of the canopy, eliminating the small leaves indicative of low expansion. Leaves were placed in paper bags and then stored in a freezer at -8°C prior to pigment determination. A 1.6 cm circle was cut out from each leaf sample for grinding in 4 ml 80% acetone, and then 8 ml acetone were added for a total of 12 ml in each tube. Tubes were stored in the dark at 4°C for 48 h prior to spectrophotometer measurements. Each sample for pigment determination was filtered and placed in a cuvette, and absorbance measured between 400 nm and 700 nm with 2 nm fixed resolution at 1 nm intervals using a Jasco V-530 UV-vis spectrophotometer (Jasco Inc., Great Dunmow, UK). Chlorophyll *a* (C_a), chlorophyll *b* (C_b), and total carotenoid (C_{x+c}) concentration were calculated using the extinction coefficients derived by Wellburn (1994), and absorbance measured at 470 nm, 646 nm, and 663 nm with Eqs. (1)–(3).

$$C_a = 12.21 \cdot A_{663} - 2.81 \cdot A_{646} \quad (1)$$

$$C_b = 20.13 \cdot A_{646} - 5.03 \cdot A_{663} \quad (2)$$

$$C_{x+c} = \frac{1000 \cdot A_{470} - 3.27 \cdot C_a - 104 \cdot C_b}{198} \quad (3)$$

A subset of leaves collected from the study sites was used to measure bands R_{515} , R_{530} and R_{570} with a customized PlantPen instrument (Photon Systems Instruments, Brno, Czech Republic). The same leaves were used to measure leaf C_{a+b} and C_{x+c} to derive relationships between the R_{515}/R_{570} and the biochemical measurements.

In addition to leaf sampling and biochemical determination, canopy structural parameters, such as grid size, number of vines within each plot, trunk height, plant height and width, and row orientation, were conducted on each $10\text{ m} \times 10\text{ m}$ plot. The leaf area index (LAI) and sunlit canopy cover in each study area were estimated using allometric methods. A summary of the structural data measured to characterize each study area is described in Table 1.

2.1.2. Airborne campaigns

Airborne campaigns were conducted in 2009 with a narrow-band multispectral camera, and in 2010 and 2011 using a micro-hyperspectral imager. Flights were undertaken using two different unmanned aerial vehicles (UAVs) operated by the Laboratory for Research Methods in Quantitative Remote Sensing (QuantaLab, IAS-CSIC, Spain) (Berni et al., 2009a; Zarco-Tejada et al., 2008, 2012).

Unmanned aerial vehicle (UAV) platforms used for remote sensing research were developed to carry payloads with thermal, multispectral and hyperspectral imaging sensors. Two UAV platforms were operated in this experiment. The first UAV consisted of a 2-m wingspan fixed-wing platform capable of 1 h endurance at 5.8 kg take-off weight (TOW) (mX-SIGHT, UAV Services and Systems, Germany). This platform was used to fly the multispectral

Table 1

Measured parameters for the vine study sites, showing the variability in row orientation, width, height and LAI.

Plot	Row orientation ($^\circ$)	Planting grid (m)	Width (m)	Height (m)	LAI
1	96.05	3×1.5	0.6	1.3	1.1
2	93.06	3×1.5	0.55	1.4	0.8
3	20.07	3×1.5	0.2	0.8	0.3
4	20.07	3×1.5	0.4	0.8	0.5
5	103.1	3×1.5	0.5	1.15	0.96
6	103.1	3×1.5	0.6	1.05	1.15
7	93.06	3×1.5	0.7	1.32	1.26
8	75.2	3×1.5	0.9	1.5	1.4
9	1.02	3×1.5	0.8	1.4	1.4
10	1.02	3×1.5	0.6	1.2	0.8
11	93.06	3×1.5	0.41	0.7	0.4
12	93.06	3×1.5	0.7	1.5	1.2
13	47.5	3×1.5	0.6	1.2	0.75
14	47.5	3×1.5	0.55	0.9	0.6
15	47.5	3×1.5	0.8	1.1	0.8
16	28.5	3×1.5	0.9	1.3	1.48
17	28.5	3×1.5	1.1	1.7	1.3
18	49.5	3×1.5	0.8	1.45	1.07
19	49.5	3×1.5	0.6	1.45	1.25
20	61.42	3×1.5	0.75	1.4	1.56
21	61.42	3×1.5	0.85	1.35	1.37

camera over the study sites in 2009, as well as to carry a thermal camera used for water stress detection as part of other studies (González-Dugo et al., 2012). A second UAV platform was developed for hyperspectral imagery acquisition, consisting of a 5-m wingspan fixed-wing platform capable of 3 h endurance at 13.5 kg take-off weight (TOW) (Viewer, ELIMCO, Seville, Spain). This larger platform enabled the acquisition of all study sites in one single flight carrying both the micro-hyperspectral imager and the thermal camera concurrently.

Both UAV platforms were controlled by an autopilot for autonomous flight (AP04, UAV Navigation, Madrid, Spain) to follow a flight plan using waypoints. The autopilot comprised a dual CPU controlling an integrated Attitude Heading Reference System (AHRS) based on a L1 GPS board, 3-axis accelerometers, gyros and a 3-axis magnetometer (Berni et al., 2009a). The ground control station and the UAV were radio linked, transmitting position, attitude and status data at 20 Hz frequency; this tunneling transmission link was also useful for communication purposes for the operation of remote sensing hyperspectral and multispectral cameras on board the UAVs.

The multispectral sensor flown in 2009 was a 6-band multispectral camera consisting of 6 independent image sensors and optics with user-configurable 10 nm full-width at half maximum (FWHM) spectral filters (Berni et al., 2009a; Zarco-Tejada et al., 2009). The image resolution was 2592×1944 pixels with 10-bit radiometric resolution, optics focal length of 8.4 mm, and angular field of view (FOV) of $38.04^\circ \times 28.53^\circ$, yielding 15 cm spatial resolution at 150 m flight altitude. The bandsets selected for this study comprised center wavelengths of 515, 530, 570, 670, 700 and 800 nm. The multispectral images acquired over each vineyard field enabled the identification of the study areas for the leaf sampling and ground structural measurements. The 2009 airborne campaign was conducted at 9:00 am GMT.

The hyperspectral imager installed on board the UAV in 2010 and 2011 was a micro-hyperspectral camera (Micro-Hyperspec VNIR model, Headwall Photonics, MA, USA) flown in the spectral mode of 260 bands at 1.85 nm/pixel and 12-bit radiometric resolution, yielding a FWHM of 3.2 nm with a 12- μm slit, and 6.4 nm with a 25- μm slit in the 400–885 nm region. Data acquisition and storage on board the UAV was set to 50 fps, and integration time was 18 ms. The 8-mm optics focal length yielded an IFOV of 0.93 mrad and an angular FOV of 50° , obtaining a swath of 522 m at $53\text{ cm} \times 42\text{ cm}$

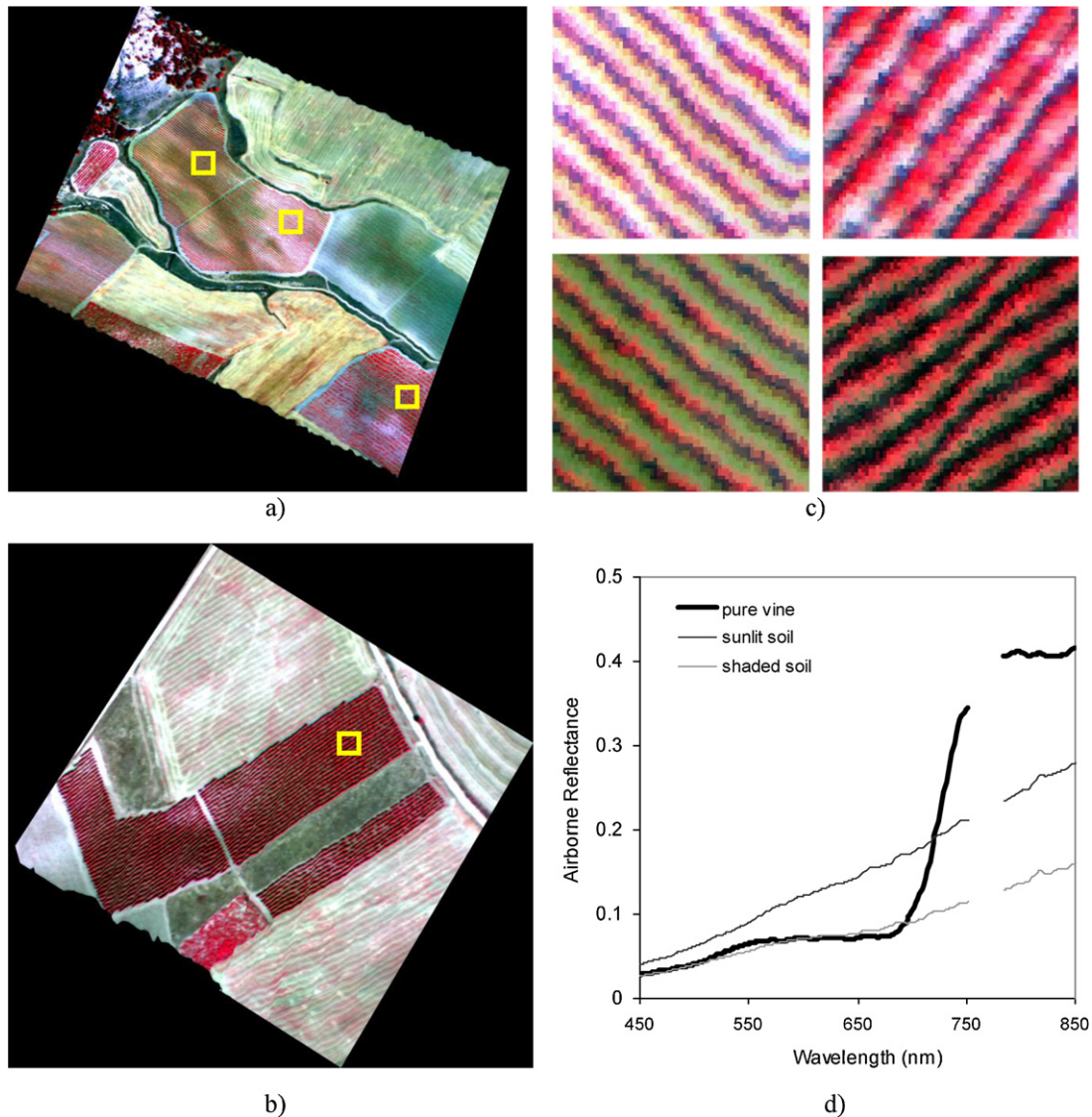


Fig. 1. Hyperspectral scene (a) obtained with the micro-hyperspectral imager on board the UAV platform at 40 cm resolution, enabling pure vine identification (b). The imagery enabled the separation of pure vine from shaded and sunlit soil reflectance (c), observing the scene components and the pure vine reflectance later used for index calculation (d). Yellow squares (a and b) shown in detail in (c). (For interpretation of the references to color in this figure legend, the reader is referred to the web version of the article.)

resolution, resampled to 40 cm for a flight conducted at 575 m AGL altitude and 75 km/h ground speed. The airborne campaigns over the vineyard fields consisted of flightlines acquired in the solar plane at 9:00 am GMT (11:00 am local time) in August 2009 using the CropSight UAV platform, and the Viewer UAV platform in 2010 and 2011. For identification purposes, each plot was marked in the field using ground control points detectable in the imagery.

The multispectral and hyperspectral sensors were radiometrically calibrated using coefficients derived in the laboratory with a calibrated uniform light source (integrating sphere, CSTM-USS-2000C Uniform Source System, LabSphere, NH, USA) at four different levels of illumination and six integration times. The atmospheric correction was conducted using total incoming irradiance at 1 nm intervals, simulated with the SMARTS model developed by the National Renewable Energy Laboratory, US Department of Energy (Gueymard, 1995, 2001), with aerosol optical depth measured at 550 nm by a Micro-Tops II sunphotometer (Solar Light Co., Philadelphia, PA, USA). Sunphotometer measurements were acquired at the time of the flights. The SMARTS model computation

for clear sky spectral irradiance was validated to match the output from the MODTRAN complex band models within 2%, but using aerosol optical depth as input. This radiative transfer model was previously used in other studies to perform the atmospheric correction of narrow-band multispectral imagery, such as in Berni et al. (2009a,b) and Suárez et al. (2010), and the atmospheric correction of the micro-hyperspectral imagery on board an UAV platform for chlorophyll fluorescence detection (Zarco-Tejada et al., 2012).

Ortho-rectification of the hyperspectral imagery acquired with the UAV platforms was conducted using PARGE (ReSe Applications Schläpfer, Wil, Switzerland) from data acquired with an inertial measuring unit (IMU) installed on board and synchronized with the hyperspectral imager. The hyperspectral imagery acquired (Fig. 1a and b) enabled pure vine identification for field validation purposes, successfully separating pure vine from shaded and sunlit soil reflectance in most cases (Fig. 1c), obtaining pure vine reflectance, sunlit and shaded soil components separately (Fig. 1d). Single vines from each vineyard field were identified using automatic object-based crown detection algorithms (Fig. 2). The

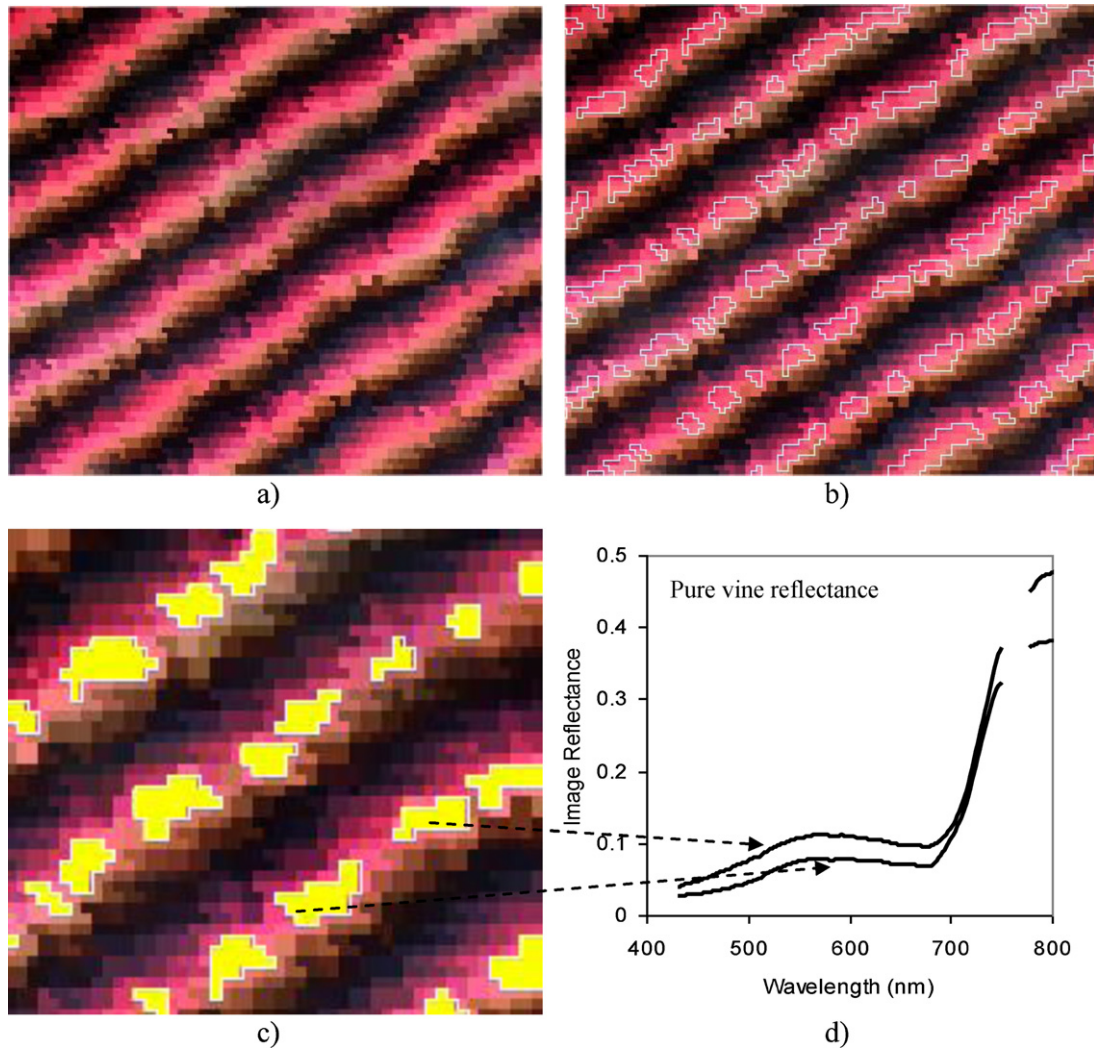


Fig. 2. Automatic object-based crown detection algorithm applied to the hyperspectral imagery acquired from the unmanned aerial vehicle (a) to identify pure vines (b and c). The methodology enabled calculation of the mean hyperspectral reflectance at the pure-vine level (d).

automatic object-based crown detection algorithm applied to the hyperspectral imagery (Fig. 2b and c) enabled calculation of the mean hyperspectral reflectance at the pure-vine level for the entire scenes acquired with the unmanned vehicle (Fig. 2d). The mean radiance and reflectance spectra calculated for each study site for the 260 spectral bands were then used for vegetation index calculation from the chlorotic and healthy study sites (some sample reflectance spectra are shown in Fig. 3).

2.2. Modeling the retrieval of carotenoid content with the R_{515}/R_{570} index

The R_{515}/R_{570} index proposed for leaf carotenoid estimation in conifer forest canopies (Hernández-Clemente et al., 2012) was investigated in this study for vineyard row-structured canopies. The PROSPECT-5 leaf radiative transfer model (Jacquemoud and Baret, 1990; Feret et al., 2008), which simulates the carotenoid and chlorophyll content effects on leaf reflectance and transmittance, was linked to canopy-level radiative transfer models, as well as to simpler approximations based on infinite reflectance (R_{∞}) formulations. The very high resolution imagery used in this study between 2009 and 2011 (15 cm resolution for the multispectral imagery, 40 cm for the hyperspectral imagery) and the pure-vine identification methods conducted on the imagery, avoiding shadows

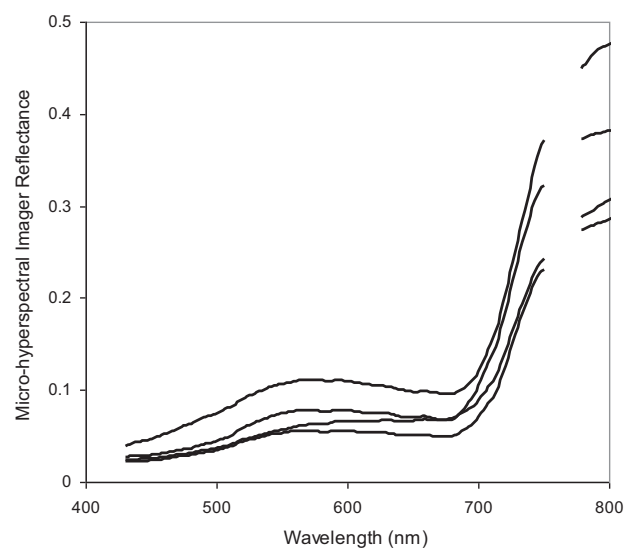


Fig. 3. Sample pure vine reflectance extracted from the imagery acquired with the micro-hyperspectral imager on board the UAV platform flown over the vineyard study sites. Reflectance spectra consisted of 260 spectral bands at 6.4 nm FWHM and 40 cm resolution.

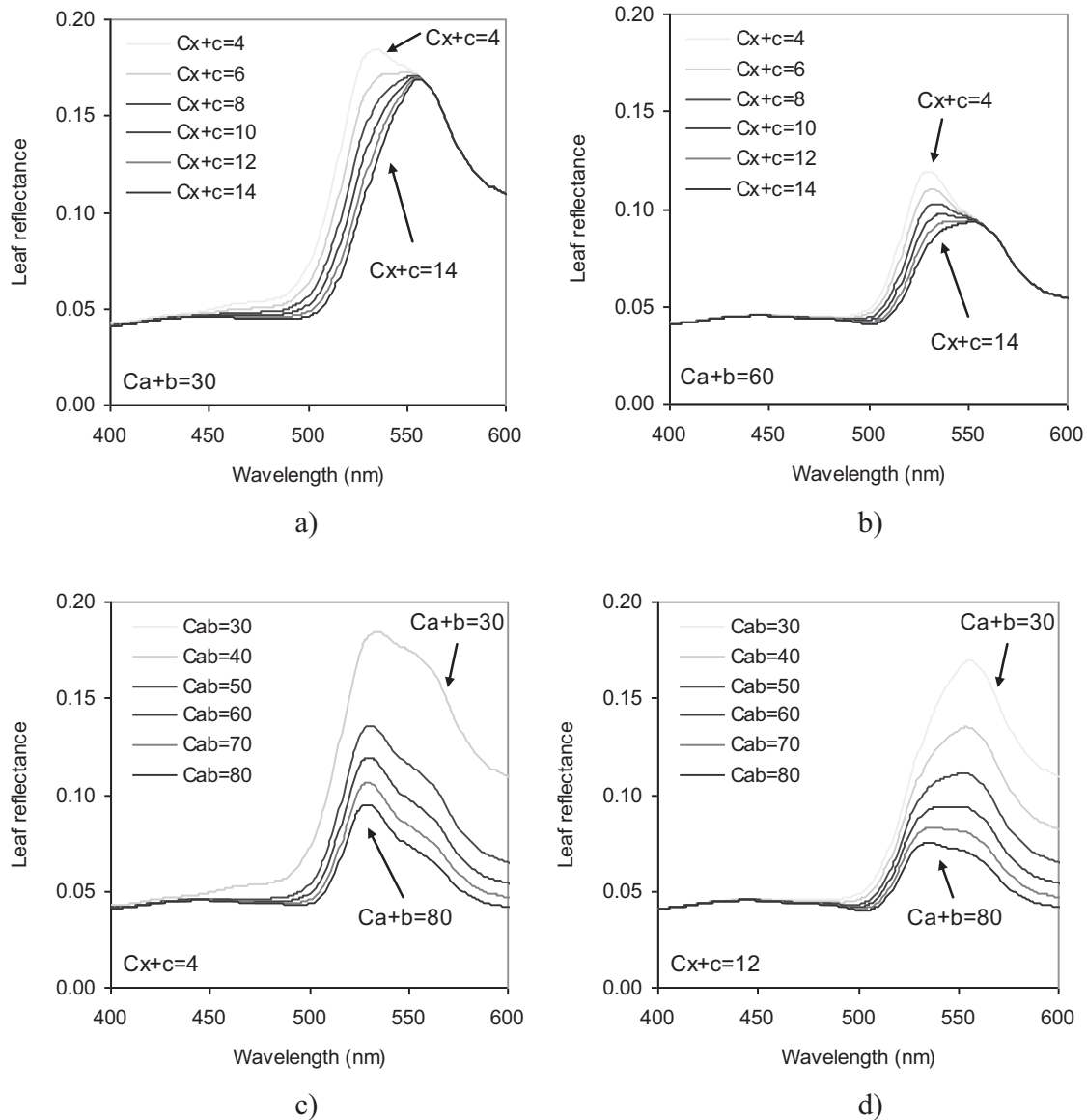


Fig. 4. Leaf-level simulations conducted with PROSPECT-5 in the 400–600 nm region for varying C_{x+c} (4–14 $\mu\text{g}/\text{cm}^2$) (a and b) and chlorophyll C_{a+b} (30–80 $\mu\text{g}/\text{cm}^2$) (c and d) for fixed $N = 1.6$, $C_w = 0.025$ cm, and $C_m = 0.03$ g/cm^2 . C_{x+c} and C_{a+b} units are in $\mu\text{g}/\text{cm}^2$.

and soil pixels, allowed the assessment of different canopy-level approximations. The retrieval capability of the leaf carotenoid content on pure vines through the R_{515}/R_{570} index was then assessed.

The PROSPECT-5 model was used to simulate leaf reflectance and transmittance for varying leaf chlorophyll C_{a+b} (30–80 $\mu\text{g}/\text{cm}^2$) and carotenoid C_{x+c} (4–14 $\mu\text{g}/\text{cm}^2$) content. The simulated leaf reflectance and transmittance spectra were used to calculate the R_{515}/R_{570} index, observing the effects caused by leaf C_{a+b} and C_{x+c} . Fig. 4 shows the effects of C_{x+c} (Fig. 4a and b) and C_{a+b} (Fig. 4c and d) on leaf reflectance for the 400–600 nm spectral region, where the proposed R_{515}/R_{570} index is calculated.

Different approaches were used to simulate the pure vine reflectance from leaf-level reflectance and transmittance spectra: (i) using simpler formulations based on infinite reflectance R_∞ simulations; and (ii) using canopy reflectance radiative transfer models. The use of different levels of complexity for simulating the pure vine reflectance was justified due to the retrieval methodology for extracting the pure vegetation pixels from the imagery, which removed or at least diminished the structural

and background effects owing to the very high spatial resolution used.

The infinite reflectance R_∞ formulations simulate the reflectance without canopy structure or viewing geometry considerations, based solely on leaf reflectance and transmittance. These R_∞ formulations simulate optically thick leaf material, assuming different multiple scattering approaches between leaf layers. This leaf-stack concept may have applicability to simulate a dense vine planted in wall-structured architectures, with little effect caused by the soil background and shadows. Nevertheless, it cannot take into consideration the viewing angle effects or the row orientation for each vineyard field under study. Comparison of the performance of these R_∞ formulations against canopy reflectance models was conducted in Zarco-Tejada et al. (2001). Different R_∞ formulations have been derived based on assumptions related to the scattering between layered leaves, expressing the optically thick medium in terms of single leaf reflectance and transmittance. Lillestaeter (1982) ($R_{\infty 1}$) (Eq. (4a)), Yamada and Fujimura (1991) ($R_{\infty 2}$) (Eq. (4b)) and Hapke (1993) ($R_{\infty 3}$) (Eq. (4c)) formulations were calculated from simulated leaf reflectance and transmittance

using PROSPECT-5. The spectra were then used to calculate the canopy-level R_{515}/R_{570} index as a function of the varying leaf inputs indicated above.

$$R_{\infty 1} = \frac{\rho}{1 - \tau^2} \quad (4a)$$

$$R_{\infty 2} = \frac{\rho}{1 - ((2\tau^2)/(1 + (1 - 4\tau^2)^{1/2}))} \quad (4b)$$

$$R_{\infty 3} = \frac{1 - \alpha^{1/2}}{1 + \alpha^{1/2}}; \quad a = 1 - r - t \quad (4c)$$

Regarding the canopy models used, a simpler radiative transfer approach was conducted with the Scattering by Arbitrary Inclined Leaves (SAIL) (Verhoef, 1984) adapted to take into account the hotspot effects or the multiple scattering in the canopy (SAILH) (Kuusk, 1985). The SAILH model approximates the canopy as a horizontally uniform parallel-plane infinitely extended medium with diffusely reflecting and transmitting elements. Although the vine canopy reflectance cannot be considered a plane-parallel canopy, the use of SAILH was justified in this study for two reasons: (i) ease of operation and calculation when linked to PROSPECT-5, which enabled the generation of synthetic spectra with low computational effort. These databases were generated in this study to assess the retrieval performance of R_{515}/R_{570} for carotenoid determination under different assumptions, including LAI variation; (ii) the methodology aimed at estimating carotenoid content from pure vine reflectance extracted after removing any shadow and soil pixel effects. Therefore, the use of the SAILH model may be valid for these high resolution pure-vine retrieval conditions. SAILH inputs were as follows: canopy architecture defined by the leaf area index (LAI) and the leaf angle distribution function (LADF), leaf reflectance and transmittance, underlying soil reflectance, and the illumination and viewing geometry (solar zenith and sensor viewing angles).

A more complex and computationally expensive approach used in this study consisted of simulating the vineyard scenes using the Monte Carlo ray tracing 3D Forest Light Interaction Model (FLIGHT) (North, 1996). The FLIGHT model was previously used to simulate row-structured canopy reflectance in olive orchards for modeling the PRI index for stress detection (Suárez et al., 2008), and peach, orange and vineyard canopies for mapping and modeling radiation interception (Guillén-Climent et al., 2012). In this study, the FLIGHT model was used to simulate the pure vine reflectance, extracting from the vineyard canopy simulation the reflectance from the center of each vine row. The 3D vineyard scene was conducted using structural inputs within the range of variation of the field data measured for each field. Input parameters defining geometrical and optical properties for the different models can be found in Table 2, showing airborne imagery acquired for two orientations (Fig. 5a and b), the FLIGHT scene generation obtained for each vineyard field (Fig. 5c and d), and the aggregated and pure vine simulated reflectance extracted from the center of the row for each scene (Fig. 5e and f).

The effects of the leaf inputs C_{a+b} , C_{x+c} , and N , the canopy parameters vine LAI, and soil reflectance were assessed within the range of variation for vineyard canopies (see Zarco-Tejada et al., 2005). Leaf inputs C_{a+b} (30–80 $\mu\text{g}/\text{cm}^2$), C_{x+c} (4–14 $\mu\text{g}/\text{cm}^2$), and N (1.6–1.8), canopy inputs LAI (1–3), and soil reflectance were ranged to calculate the proposed R_{515}/R_{570} index.

Scaling up relationships linking PROSPECT-5 and the different approximations proposed for simulating the vine reflectance were conducted: (i) the three infinite reflectance R_{∞} formulations ($R_{\infty 1}$, $R_{\infty 2}$, $R_{\infty 3}$); (ii) SAILH; and (iii) FLIGHT. A synthetic spectra database was generated using 1000 random inputs for leaf C_{a+b} and C_{x+c} for the ranges indicated, C_m (0–0.03), N (1.6–1.8), LAI (1–3), and soil reflectance variation. The database was used to develop each

Table 2

Nominal values and range of parameters used for leaf and canopy simulation with PROSPECT-5, SAILH and FLIGHT for pure vine reflectance simulation.

	Nominal values and range
PROSPECT	
Chlorophyll $a+b$, C_{a+b} ($\mu\text{g}/\text{cm}^2$)	30–80
Carotenoid content, C_{x+c} ($\mu\text{g}/\text{cm}^2$)	4–14
Leaf water content, C_w (cm)	0.025
Leaf dry matter content, C_m (g/cm^2)	0.03
Leaf internal structure parameter, N	1.6–1.8
SAILH	
Leaf reflectance and transmittance	PROSPECT-5 simulations
Soil reflectance	Random (0–1)
Leaf area index	1–3
Leaf angle distribution function	$\varepsilon = 0.95$; $\theta_n = 45^\circ$ (plagiophile)
Viewing geometry (θ_s , θ_v , ϕ)	Calculated for each image and site
Hotspot parameter	0.083
FLIGHT	
Hemispherical reflectance and transmittance of green leaves	PROSPECT-5 simulations
Hemispherical reflectance and transmittance of senescent leaves	Not used
Leaf equivalent radius	0.083 m
Leaf area index (LAI)	1–3
Fractional cover	Estimated from Table 1
Leaf angle distribution function (LADF)	Plagiophile
Fraction of green leaves	1
Fraction of senescent leaves	0
Fraction of bark	0
Number of stands and position coordinates	Not used
Crown shape	Elliptical
Crown height and radius	From Table 1 (m)
Trunk height and radius	Field measured
Viewing geometry angles	Calculated for each image and site
Soil reflectance	From image
Soil roughness	0
Aerosol optical depth (AOD)	Measured at the time of flights

relationship (500 samples), using the remaining 500 samples to calculate the coefficient of determination and the RMSE for each scaling up approach developed using R_{∞} , SAILH and FLIGHT canopy reflectance simulation approaches. The scaling up modeling method aimed at estimating leaf C_{x+c} independently from C_{a+b} . The relationships were based on five different case scenarios that used the R_{515}/R_{570} index only as a proxy for C_{x+c} as well as the combination of both the R_{515}/R_{570} (sensitive to C_{x+c}) and TCARI/OSAVI (sensitive to C_{a+b}) for a more accurate retrieval of leaf carotenoid content. In particular, Cases 1–4 consisted of estimating leaf C_{x+c} using models based on the R_{515}/R_{570} index only, while Case 5 included both the R_{515}/R_{570} (sensitive to C_{x+c}) and TCARI/OSAVI (sensitive to C_{a+b}) in the estimation of C_{x+c} . Cases 1 and 2 were based on fixed C_{a+b} values, while Cases 3–5 allowed C_{a+b} to vary randomly. Cases 4 and 5 allowed variation of all inputs; the only difference between Case 4 and Case 5 is that the latter used both the R_{515}/R_{570} and TCARI/OSAVI indices to estimate leaf C_{x+c} , while the former (Case 4) used only the R_{515}/R_{570} .

These methods used to simulate random synthetic spectra from inputs and ranges indicated in Table 2 enabled building prediction relationships in the form $C_{x+c} = f(R_{515}/R_{570}; R_{515}/R_{570}^2; \text{TCARI/OSAVI})$. The algorithms were developed for each model approach through scaling up simulations conducted with PROSPECT-5 linked to the three infinite reflectance formulations ($R_{\infty 1}$; $R_{\infty 2}$; $R_{\infty 3}$), SAILH, and FLIGHT. The leaf C_{x+c} estimated from the imagery with each simulation approach was then compared against field-measured carotenoid content data measured by destructive sampling from each study site, calculating the RMSE and the relative RMSE (R-RMSE) according to Kroll and Stedinger (1996).

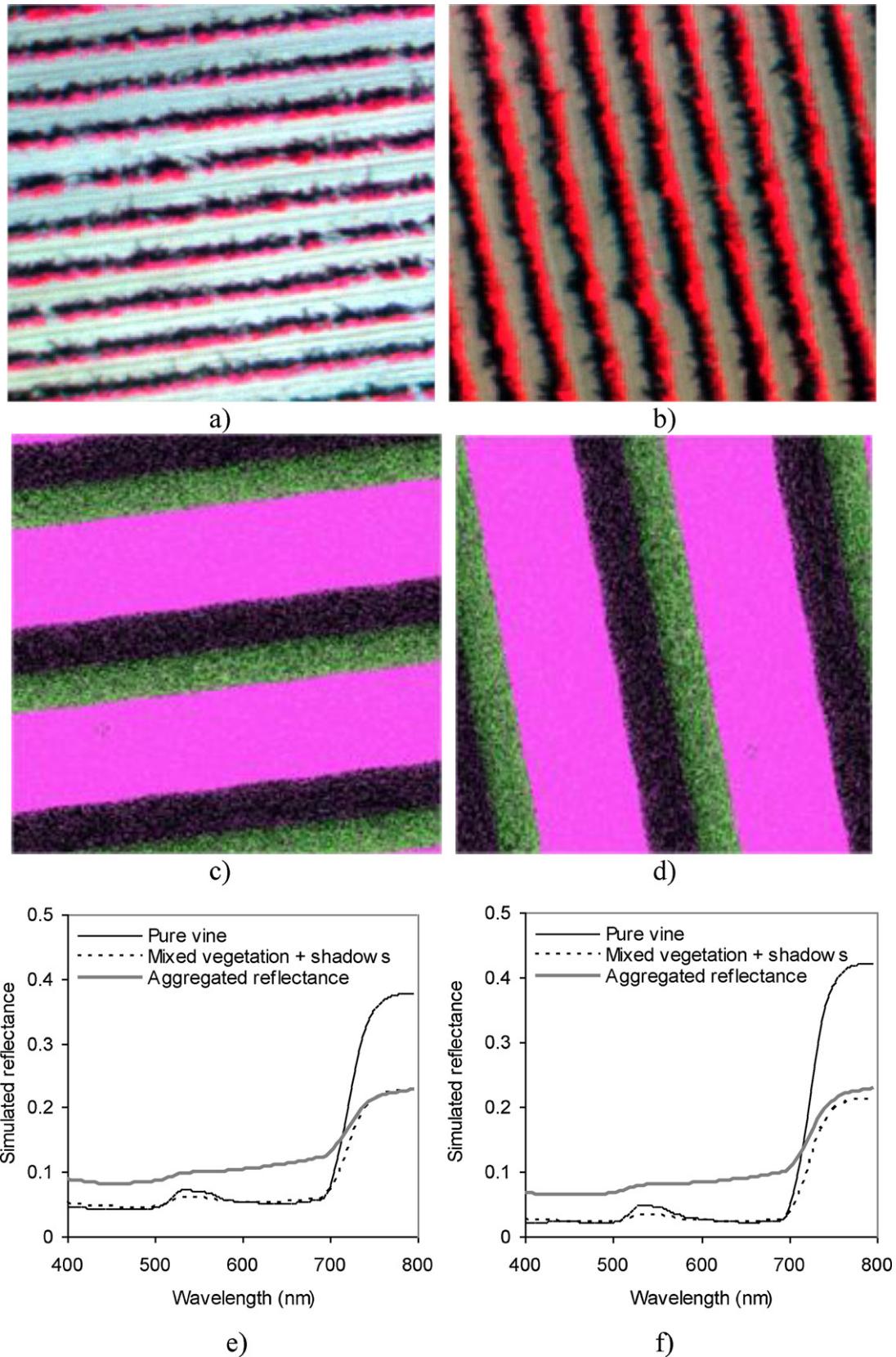


Fig. 5. Images acquired by the hyperspectral imager on board the UAV platform over two vineyards with opposite row orientation (a and b), showing the corresponding simulated scene generation with FLIGHT (c and d). The simulated canopy reflectance extracted from the center of the row and aggregated scenes are shown (e and f).

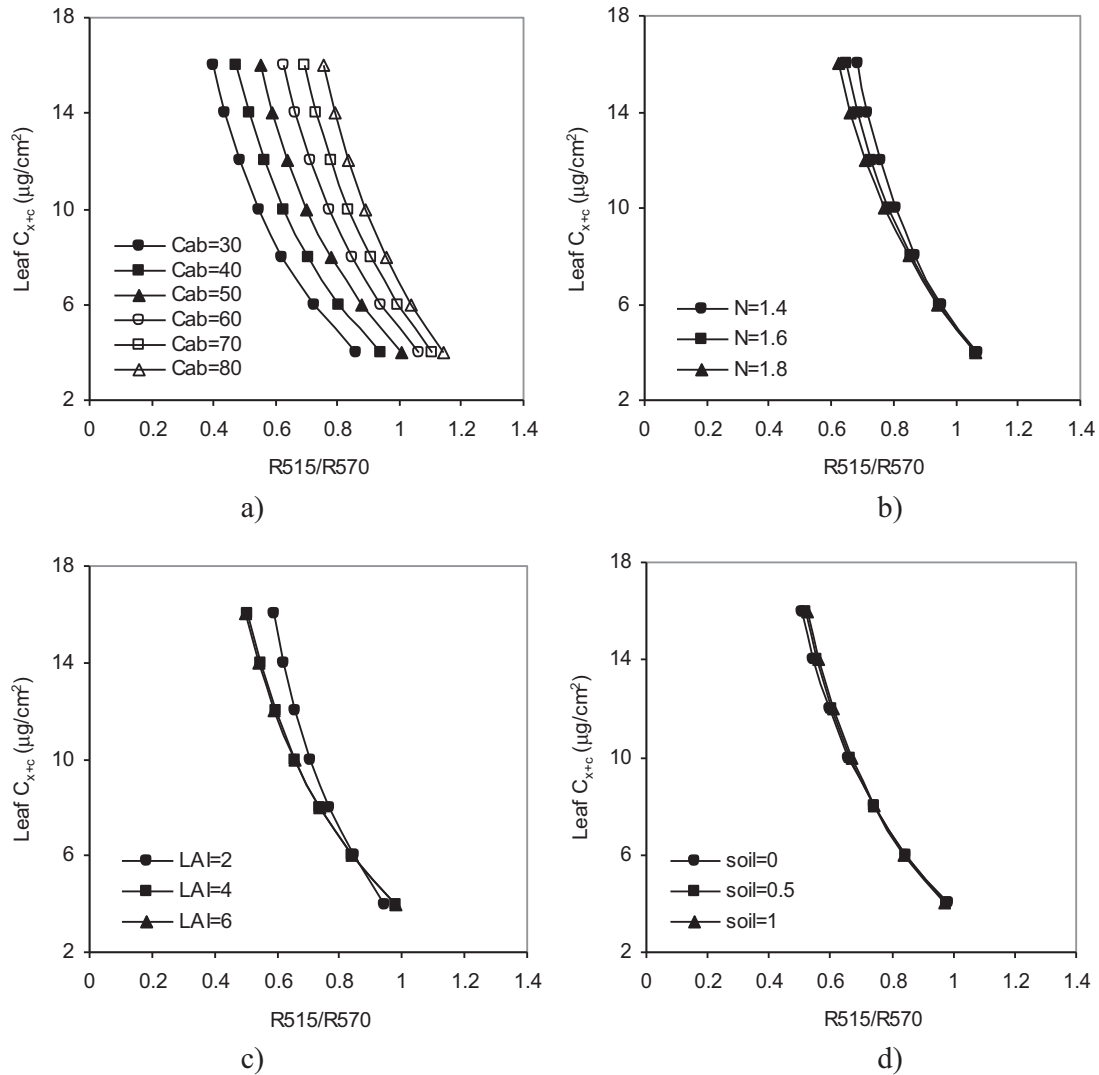


Fig. 6. Modeling results achieved with PROSPECT-5 + SAILH for R_{515}/R_{570} and leaf C_{x+c} as a function of leaf C_{a+b} content (a), leaf N parameter (b), LAI (c) and soil reflectance variation (d).

3. Results

3.1. Modeling results

Modeling results achieved with PROSPECT-5 linked to SAILH demonstrated a relationship between R_{515}/R_{570} and leaf C_{x+c} as a function of C_{a+b} (Fig. 6a), with little effect caused by the leaf N parameter (Fig. 6b), LAI (Fig. 6c) and insensitivity to soil reflectance variation (Fig. 6d). The simulations demonstrated that a family of relationships exists as a function of chlorophyll concentration, thus making it important to account for C_{a+b} when estimating leaf C_{x+c} . As an example, simulation results suggested that the same R_{515}/R_{570} index value ($R_{515}/R_{570} = 0.7$) could be related to C_{x+c} ranging between 6 and 15 $\mu\text{g}/\text{cm}^2$ when C_{a+b} is set to 30 $\mu\text{g}/\text{cm}^2$ or 60 $\mu\text{g}/\text{cm}^2$ (Fig. 6a).

The simulation study conducted with PROSPECT-5 and the different canopy approximations through infinite reflectance R_{∞} formulations and SAILH is summarized in Table 3. The synthetic spectra database generated using 1000 random inputs for C_{a+b} , C_{x+c} , N, LAI, soil reflectance and C_m yielded different coefficients of determination and RMSE values as a function of the scenarios studied (Cases 1–5) and simulation model used.

The modeling methods demonstrated that lower coefficients of determination and higher RMSE values were obtained when C_{a+b} was randomly varied and only R_{515}/R_{570} was used to estimate leaf C_{x+c} ($r^2 = 0.51$; RMSE = 1.99 $\mu\text{g}/\text{cm}^2$ for PROSPECT+SAILH). However, when all parameters were allowed to vary randomly and C_{x+c} was estimated using both R_{515}/R_{570} and TCARI/OSAVI indices, the coefficients of determination increased and RMSE decreased substantially ($r^2 = 0.93$; RMSE = 0.73 $\mu\text{g}/\text{cm}^2$ for PROSPECT+SAILH). These simulation results using synthetic spectra confirmed that estimating leaf C_{x+c} with both R_{515}/R_{570} and TCARI/OSAVI yielded the best results due to the combined contribution of both R_{515}/R_{570} (sensitive to C_{x+c}) and TCARI/OSAVI (sensitive to C_{a+b}).

Among the canopy models proposed, results obtained with the synthetic spectra database showed that $R_{\infty 1}$ and $R_{\infty 3}$ outperformed $R_{\infty 2}$. The SAILH model yielded an RMSE of 0.73 $\mu\text{g}/\text{cm}^2$, obtaining a performance close to $R_{\infty 1}$ (0.58 $\mu\text{g}/\text{cm}^2$) and $R_{\infty 3}$ (0.46 $\mu\text{g}/\text{cm}^2$). The higher error obtained with SAILH as compared to $R_{\infty 2}$ models was due to the effects caused by random LAI on the retrieval of leaf C_{x+c} from the synthetic spectra. This result is consistent as R_{∞} formulations lack input parameters related to the canopy structure. The next section shows the results obtained for leaf C_{x+c} estimation when the methodology based on R_{515}/R_{570} and TCARI/OSAVI was

Table 3
Simulation study conducted with PROSPECT-5 and different canopy approximations through infinite reflectance R_{∞} formulations and SAILH.

	PROSPECT-5 + $R_{\infty 1}$		PROSPECT-5 + $R_{\infty 2}$		PROSPECT-5 + $R_{\infty 3}$		PROSPECT-5 + SAILH	
	R^2	RMSE ($\mu\text{g}/\text{cm}^2$)	R^2	RMSE ($\mu\text{g}/\text{cm}^2$)	R^2	RMSE ($\mu\text{g}/\text{cm}^2$)	R^2	RMSE ($\mu\text{g}/\text{cm}^2$)
Case 1 $C_{x+c}^a, C_{a+b}, N, \text{LAI}, \rho_{\text{soil}}$	0.99	0.08	0.99	0.06	0.99	0.07	0.99	0.08
Case 2 $C_{x+c}^a, C_{a+b}, N^a, \text{LAI}^a, \rho_{\text{soil}}^a$	0.99	0.15	0.98	0.33	0.99	0.07	0.98	0.29
Case 3 $C_{x+c}^a, C_{a+b}^a, N, \text{LAI}, \rho_{\text{soil}}$	0.51	1.97	0.74	1.46	0.61	1.78	0.5	1.99
Case 4 $C_{x+c}^a, C_{a+b}^a, N^a, \text{LAI}^a, \rho_{\text{soil}}^a$	0.54	1.97	0.72	1.56	0.62	1.83	0.51	1.99
Case 5 $C_{x+c}^a, C_{a+b}^a, N^a, \text{LAI}^a, \rho_{\text{soil}}^a$	0.96	0.58	0.73	1.49	0.97	0.46	0.93	0.73

Cases 1–4 are models $C_{x+c} = f(R_{515}/R_{570})$.

Case 5 are models with C_{x+c} (R_{515}/R_{570}) and C_{a+b} (TCARI/OSAVI) indices: $C_{x+c} = f(R_{515}/R_{570}; R_{515}/R_{570}^2; \text{TCARI/OSAVI})$.

^a Parameters allowed varying randomly.

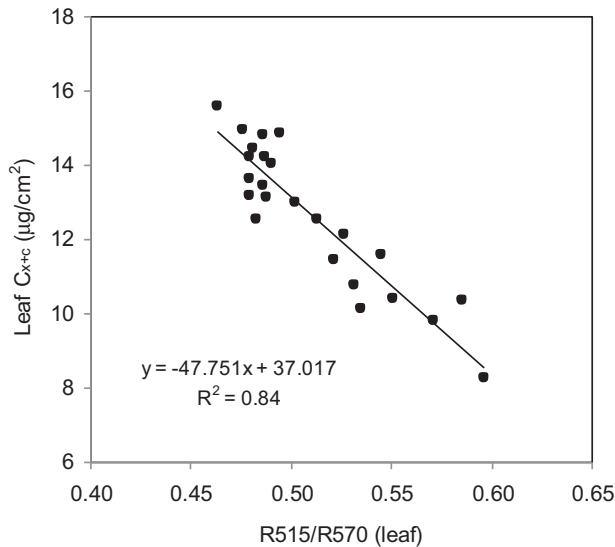


Fig. 7. Relationship obtained at the leaf level between the R_{515}/R_{570} index measured with the customized PlantPen instrument (Photon Systems Instruments, Brno, Czech Republic) and leaf C_{x+c} measured by destructive sampling.

applied to imagery acquired in 2009–2011 using infinite reflectance formulations, SAILH, and the 3D Monte Carlo FLIGHT model.

3.2. Experimental results

The leaf-level measurements conducted with the PlantPen instrument (Photon Systems Instruments, Brno, Czech Republic) customized for carotene estimation with R_{515} and R_{570} bands showed a good relationship ($r^2 = 0.84$) between the R_{515}/R_{570} index and leaf C_{x+c} measured by destructive sampling (Fig. 7). This result obtained at the leaf level confirms the previous modeling conclusions, which demonstrated the sensitivity of the R_{515}/R_{570} index to leaf C_{x+c} content.

The relationship between the R_{515}/R_{570} and leaf C_{x+c} calculated from the airborne imagery demonstrated consistent results for the 3 years of the study (Fig. 8), yielding r^2 values in the range of 0.43–0.48, which were statistically significant ($p < 0.01$ for the 3

Table 4
Coefficients of determination and RMSE obtained for 3 years of airborne imagery for leaf C_{x+c} estimation with models built as $C_{x+c} = f(R_{515}/R_{570}; R_{515}/R_{570}^2; \text{TCARI/OSAVI})$ obtained through *scaling up*. Simulations were conducted with PROSPECT-5 linked to infinite reflectance ($R_{\infty 1}; R_{\infty 2}; R_{\infty 3}$), SAILH and FLIGHT.

	PROSPECT-5 + $R_{\infty 1}$		PROSPECT-5 + $R_{\infty 2}$		PROSPECT-5 + $R_{\infty 3}$		PROSPECT-5 + SAILH		PROSPECT-5 + FLIGHT	
	R^2	RMSE ($\mu\text{g}/\text{cm}^2$)	R^2	RMSE ($\mu\text{g}/\text{cm}^2$)	R^2	RMSE ($\mu\text{g}/\text{cm}^2$)	R^2	RMSE ($\mu\text{g}/\text{cm}^2$)	R^2	RMSE ($\mu\text{g}/\text{cm}^2$)
$C_{x+c} = f(R_{515}/R_{570};$	0.28	2.4	0.41	1.6	0.19	4.4	0.2	4.6	0.26	2.91
$R_{515}/R_{570}^2;$	0.59	3.4	0.64	0.94	0.56	1.08	0.56	1.28	0.58	1.32
TCARI/OSAVI)	0.44	3.2	0.44	0.8	0.28	0.93	0.44	1.08	0.55	1.25

years). The TCARI/OSAVI index was also related to leaf C_{a+b} with similar results ($r^2 = 0.51; p < 0.001$ for years 2010 and 2011) (Fig. 9), consistent with previously published studies that assessed the sensitivity of the TCARI/OSAVI to C_{a+b} in vineyards (Zarco-Tejada et al., 2005).

The methodology described earlier was used to estimate leaf C_{x+c} from hyperspectral imagery using the *scaling up* algorithm $C_{x+c} = f(R_{515}/R_{570}; R_{515}/R_{570}^2; \text{TCARI/OSAVI})$ through each model approach, linking PROSPECT-5 to infinite reflectance formulations ($R_{\infty 1}; R_{\infty 2}; R_{\infty 3}$), SAILH, and FLIGHT (Table 4). The best results for the 3 years were found for $R_{\infty 2}$ ($r^2 = 0.41–0.64$), SAILH ($r^2 = 0.2–0.56$) and FLIGHT ($r^2 = 0.26–0.58$). The lowest RMSE errors were obtained for the $R_{\infty 2}$ model (RMSE = 0.8–1.6 $\mu\text{g}/\text{cm}^2$; R-RMSE = 8.9–15%, while FLIGHT performed better (RMSE = 1.25–2.91 $\mu\text{g}/\text{cm}^2$; R-RMSE = 14.0–29.2%) than SAILH (RMSE = 1.08–4.6 $\mu\text{g}/\text{cm}^2$; R-RMSE = 12.4–37.5%). Most errors were obtained when estimating C_{x+c} from the 2009 imagery (multispectral imagery acquired from the multi-lens camera), while 2010 and 2011 (hyperspectral imagery) yielded lower RMSE values (RMSE < 1 $\mu\text{g}/\text{cm}^2$ for $R_{\infty 2}$ (9.7%) and RMSE < 1.3 $\mu\text{g}/\text{cm}^2$ for the SAILH (12.9%) and FLIGHT (14.4%) models).

Results obtained when estimating leaf C_{x+c} from combined 2010+2011 hyperspectral imagery showed larger errors when using the $R_{\infty 1}$ formulation (RMSE = 3.23 $\mu\text{g}/\text{cm}^2$; 35.8%) as compared to $R_{\infty 2}$ (RMSE = 0.87 $\mu\text{g}/\text{cm}^2$; 9.7%) (Fig. 10a). Retrieval from SAILH and FLIGHT (Fig. 10b) yielded similar results for both models (RMSE < 1.3 $\mu\text{g}/\text{cm}^2$), with R-RMSE errors of 14.4% (FLIGHT) and 12.9% (SAILH) but slopes closer to 1:1 than in R_{∞} models.

This methodology was applied at the vine level to two sample vineyard fields, estimating leaf C_{x+c} with both the R_{515}/R_{570} and TCARI/OSAVI indices acquired from the hyperspectral imager on board the unmanned aerial vehicle (Fig. 11). The hyperspectral imagery acquired (Fig. 11a and c) enabled the estimation of leaf C_{x+c} at the vine level for the entire scene (Fig. 11b and d), assessing the within-field spatial variability of carotenoid content at the vineyard field. Leaf carotenoid content was estimated in pure vegetation pixels only (vine level) with soil and shadows removed. This provided an interpolated continuous map of leaf C_{x+c} for the entire vineyard. The maps show the spatial patterns of leaf carotenoid content regardless of chlorophyll content and within-field spatial variability of vine LAI.

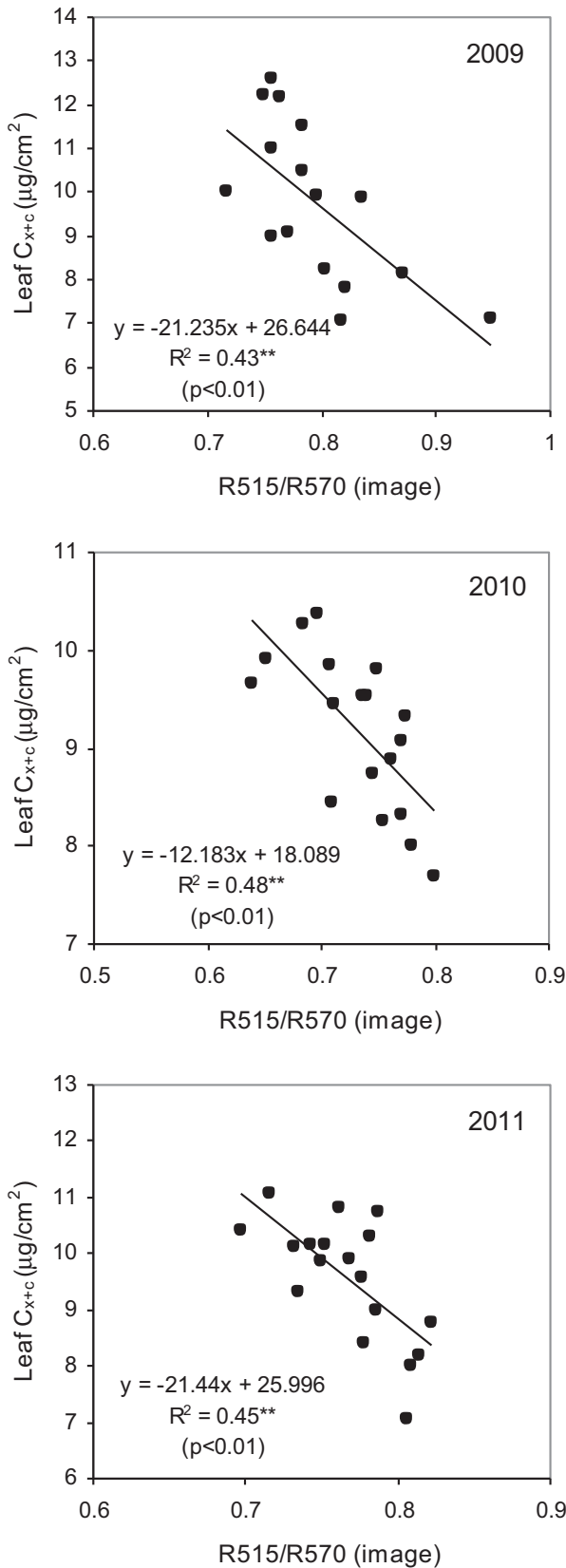


Fig. 8. Relationships obtained between the R_{515}/R_{570} index calculated for each vineyard site from the airborne hyperspectral imagery and leaf C_{x+c} measured in the field for the 3 years under study.

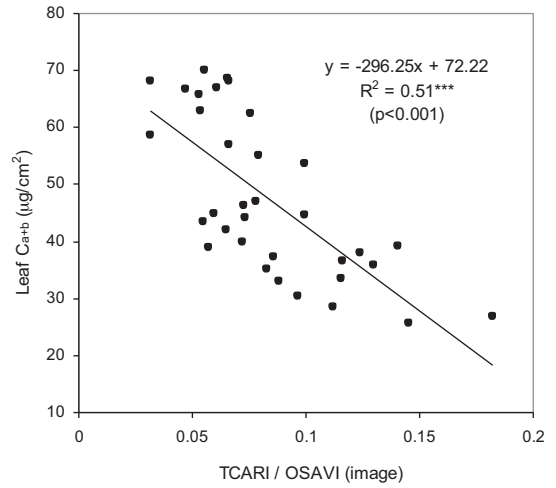


Fig. 9. Relationship obtained between the TCARI/OSAVI index calculated for each vineyard site from the airborne hyperspectral imagery and leaf C_{a+b} measured in the field for years 2010 and 2011.

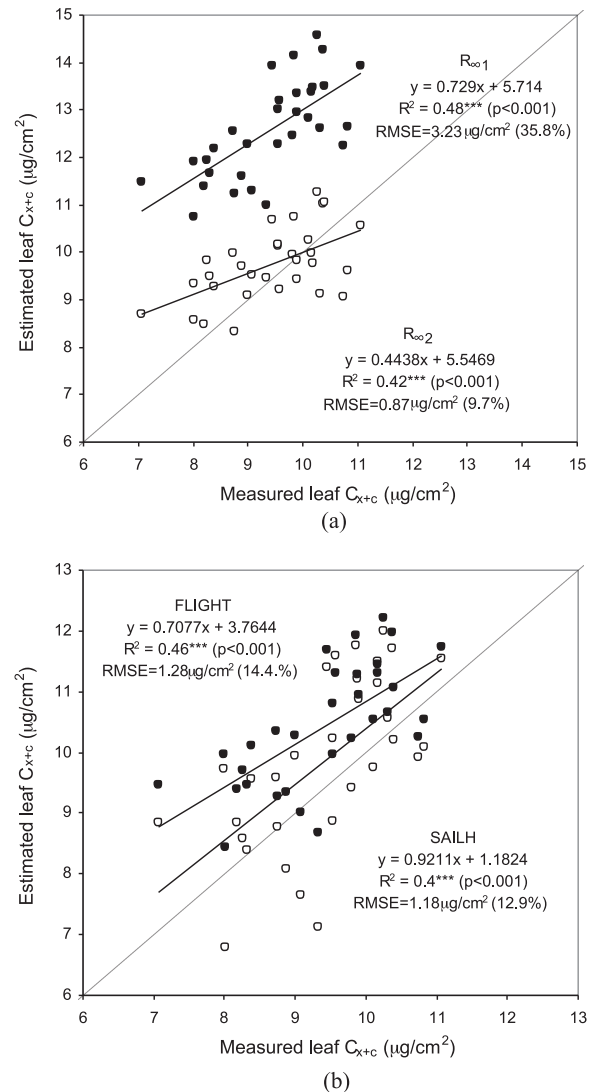


Fig. 10. Validation results obtained for the estimation of leaf C_{x+c} from the airborne hyperspectral imagery for 2010 and 2011 using R_{515}/R_{570} and TCARI/OSAVI with infinite reflectance formulations (a), SAILH and FLIGHT (b).

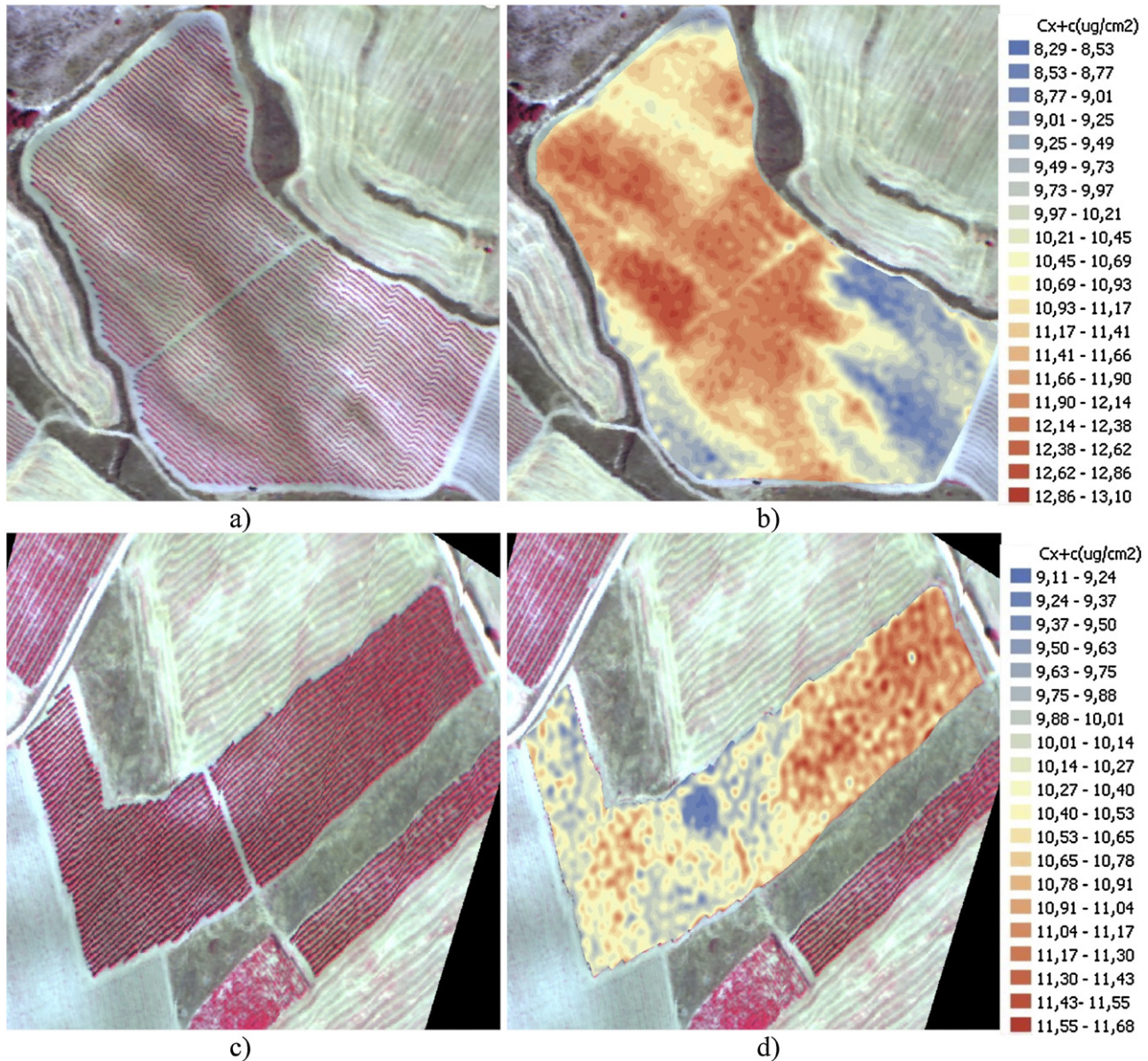


Fig. 11. Mapping results obtained on two sample vineyard fields (a and c) with the hyperspectral imager on board the unmanned aerial vehicle. Leaf C_{x+c} content was estimated from the R_{515}/R_{570} and TCARI/OSAVI indices using FLIGHT.

4. Conclusions

Modeling and experimental results obtained in this study demonstrated that estimating leaf carotenoid content in vineyards using hyperspectral imagery was feasible, yielding errors below $1 \mu\text{g}/\text{cm}^2$ (9.7% relative error) when using high resolution hyperspectral imagery. The analysis was conducted with simpler approximations based on infinite reflectance formulations (Hapke, Lillistaeter, and Yamada and Fujimura), and with canopy models such as SAILH and FLIGHT linked to PROSPECT-5. This simulated the effects of varying leaf chlorophyll content, leaf structure, canopy LAI, and soil reflectance on the retrieval of carotenoid content at the vine level using the R_{515}/R_{570} index. Simulation results demonstrated that higher accuracy for leaf C_{x+c} estimation is obtained when the retrieval is conducted simultaneously with an index sensitive to leaf C_{a+b} content, such as the TCARI/OSAVI. Therefore, this methodology combines the R_{515}/R_{570} and TCARI/OSAVI indices to enable an independent estimation of leaf carotene

content, reducing the effects of chlorophyll on the R_{515}/R_{570} index. Modeling results obtained with synthetic spectra suggested that leaf C_{x+c} can be retrieved with $r^2 = 0.93$ and $\text{RMSE} = 0.73 \mu\text{g}/\text{cm}^2$ when both R_{515}/R_{570} and TCARI/OSAVI indices are used to build the *scaling up* relationships developed through infinite reflectance and canopy simulation models.

Experimental results achieved at the leaf level and from the 3 years of multispectral and hyperspectral airborne flights using an unmanned aerial vehicle confirmed the modeling results obtained with synthetic spectra simulations assessed under different scenarios. The results demonstrated the sensitivity of the R_{515}/R_{570} index to field-measured C_{x+c} content at the leaf level ($r^2 = 0.84$) and at the airborne level, yielding errors below $1.3 \mu\text{g}/\text{cm}^2$ for the 2 years of hyperspectral imagery. Scaling up methods that used simpler approaches, such as the infinite reflectance formulation by Yamada and Fujimura, yielded better results than more complex canopy models such as SAILH and FLIGHT. The performance of these dark-dense approximations was comparable to that of radiative transfer

methods because very high spatial resolution was used in this study (40 cm resolution) to extract pure vine reflectance from the hyperspectral imagery, removing mixed pixels and soil effects. Under such conditions, leaf C_{x+c} estimates using the combined indices R_{515}/R_{570} (sensitive to C_{x+c}) and TCARI/OSAVI (sensitive to C_{a+b}) yielded RMSE values for $R_{\infty 2}$ below $0.9 \mu\text{g}/\text{cm}^2$ (9.7%), while FLIGHT ($1.28 \mu\text{g}/\text{cm}^2$) and SAILH ($1.18 \mu\text{g}/\text{cm}^2$) obtained relative errors of 14.4% and 12.9% for the 2 years of hyperspectral imagery. The better performance of $R_{\infty 2}$ when compared to SAIL was due to the limitations of the latter to simulate pure-vine dense canopy reflectance, as observed in Fig. 6c. The saturation effects found in the relationship between leaf C_{x+c} and canopy R_{515}/R_{570} for LAI values above 3 played a critical role in the performance of plane-parallel approximations for vineyards based on SAIL. Nevertheless, estimations conducted with SAILH and FLIGHT obtained model slopes closer to the 1:1 line than those using R_{∞} models.

Results obtained for 2010 and 2011 with hyperspectral imagery yielded lower RMSE values than estimates conducted with multispectral imagery (2009). A reason for this may be that the indices calculated with multispectral imagery included pixel mismatches between bands that are inherent to the miniaturized multi-lens camera technology used in most UAVs and have important effects on the spectral indices calculated.

In summary, the results obtained over the 3 years of the study demonstrate that maps of the spatial variability of leaf carotenoid content in vineyards can be obtained with errors below $1 \mu\text{g}/\text{cm}^2$ (9.7%) using a micro-hyperspectral imager on board an unmanned aerial vehicle to warrant high spatial resolution imagery. The very high spatial resolution obtained (40 cm pixel size), along with rich 260-band spectral information of 6.4 nm FWHM at 1.85 nm/pixel sampling, enabled the generation of leaf C_{x+c} maps using the combined R_{515}/R_{570} and TCARI/OSAVI indices for their application in precision agriculture and physiological condition monitoring.

Acknowledgements

Financial support from the Spanish Ministry of Science and Education (MEC) for the AGL2009-13105 project and FEDER funding are gratefully acknowledged. Technical support from Headwall Photonics, UAV Navigation, Tetracam, UAV Services and Systems, and ELIMCO for the accommodation of airborne requirements, camera support and UAV platform developments is also acknowledged. D. Notario, A. Vera, A. Hornero, and R. Romero are acknowledged for technical support during field and airborne campaigns. The scientific and editorial comments of V. Gonzalez-Dugo and B. Markowitz are appreciated.

References

- Berni, J.A.J., Zarco-Tejada, P.J., Suárez, L., Fereres, E., 2009a. Thermal and narrow-band multispectral remote sensing for vegetation monitoring from an unmanned aerial vehicle. *IEEE Trans. Geosci. Remote Sens.* 47 (3), 722–738.
- Berni, J.A.J., Zarco-Tejada, P.J., Sepulcre-Cantó, G., Fereres, E., Villalobos, F.J., 2009b. Mapping canopy conductance and CWSI in olive orchards using high resolution thermal remote sensing imagery. *Remote Sens. Environ.* 113, 2380–2388.
- Blackburn, G.A., 1998. Quantifying chlorophylls and carotenoids at leaf and canopy scales: an evaluation of some hyperspectral approaches. *Remote Sens. Environ.* 66, 273–285.
- Carter, G.A., Spiering, B.A., 2002. Optical properties of intact leaves for estimating chlorophyll concentration. *J. Environ. Qual.* 31 (5), 1424–1432.
- Chappelle, E.W., Kim, M.S., McMurtrey, J.E.I., 1992. Ratio analysis of reflectance spectra (RARS): an algorithm for the remote estimation of the concentrations of chlorophyll a, chlorophyll b, and carotenoids in soybean leaves. *Remote Sens. Environ.* 39, 239–247.
- Demmig-Adams, B., Adams III, W.W., 1992. Photoprotection and other responses of plants to high light stress. *Annu. Rev. Plant Physiol. Plant Mol. Biol.* 43, 599–626.
- Demmig-Adams, B., 1998. Survey of thermal energy dissipation and pigment composition in sun and shade leaves. *Plant Cell Physiol.* 39, 474–482.
- Feret, J.B., François, C., Asner, G.P., Gitelson, A.A., Martin, R., Bidel, L.P.R., 2008. PROSPECT-4 and 5: advances in the leaf optical properties model separating photosynthetic pigments. *Remote Sens. Environ.* 112, 3030–3043.
- Feret, J.B., François, C., Gitelson, A., Asner, G.P., Barry, K.M., Panigada, C., Richardson, A.D., Jacquemoud, S., 2011. Optimizing spectral indices and chemometric analysis of leaf chemical properties using radiative transfer modeling. *Remote Sens. Environ.* 115 (10), 2742–2750.
- Frank, H.A., Cogdell, R.J., 1996. Carotenoids in photosynthesis. *Photochem. Photobiol.* 63, 257–264.
- Gamon, J.A., Peñuelas, J., Field, C.B., 1992. A narrow-waveband spectral index that tracks diurnal changes in photosynthetic efficiency. *Remote Sens. Environ.* 41, 35–44.
- Garrity, S.R., Eitel, J.U.H., Vierling, L.A., 2011. Disentangling the relationships between plant pigments and the photochemical reflectance index reveals a new approach for remote estimation of carotenoid content. *Remote Sens. Environ.* 115, 628–635.
- Gitelson, A.A., Zur, Y., Chivkunova, O.B., Merzlyak, M.N., 2002. Assessing carotenoid content in plant leaves with reflectance spectroscopy. *J. Photochem. Photobiol. B: Biol.* 75, 272–281.
- Gitelson, A.A., Gritz, Y., Merzlyak, M.N., 2003. Relationships between leaf chlorophyll content and spectral reflectance and algorithms for nondestructive chlorophyll assessment in higher plants. *J. Plant Physiol.* 160 (3), 271–282.
- González-Dugo, V., Zarco-Tejada, P.J., Berni, J.A., Suarez, L., Goldhamer, D., Fereres, E., 2012. Almond tree canopy temperature reveals intra-crown variability that is water stress-dependent. *Agric. Forest Meteorol.* 154–155, 156–165.
- Gueymard, C.A., 1995. SMARTS, A Simple Model of the Atmospheric Radiative Transfer of Sunshine: Algorithms and Performance Assessment. Technical Report No. FSECPF-270-95. Florida Solar Energy Center, Cocoa, FL.
- Gueymard, C.A., 2001. Parameterized transmittance model for direct beam and circumsolar spectral irradiance. *Solar Energy* 71, 325–346.
- Guillén-Climent, M.L., Zarco-Tejada, P.J., Berni, J.A.J., North, P.R.J., Villalobos, F.J., 2012. Mapping radiation interception in row-structured orchards using 3D simulation and high resolution airborne imagery acquired from an UAV. *Prec. Agric.* 13, 473–500.
- Haboudane, D., Miller, J.R., Pattey, E., Zarco-Tejada, P.J., Strachan, I., 2004. Hyperspectral vegetation indices and novel algorithms for predicting green LAI of crop canopies: modeling and validation in the context of precision agriculture. *Remote Sens. Environ.* 90 (3), 337–352.
- Haboudane, D., Miller, J.R., Tremblay, N., Zarco-Tejada, P.J., Dextraze, L., 2002. Integration of hyperspectral vegetation indices for prediction of crop chlorophyll content for application to precision agriculture. *Remote Sens. Environ.* 81 (2/3), 416–426.
- Hapke, B., 1993. *Theory of Reflectance and Emittance Spectroscopy*. Univ. Press, Cambridge, UK.
- Hernández-Clemente, R., Navarro-Cerrillo, R., Suárez, L., Morales, F., Zarco-Tejada, P.J., 2011. Assessing structural effects on PRI for stress detection in conifer forests. *Remote Sens. Environ.* 115 (9), 2360–2375.
- Hernández-Clemente, R., Navarro-Cerrillo, R.M., Zarco-Tejada, P.J., 2012. Carotenoid content estimation in a heterogeneous conifer forest using narrow-band indices and PROSPECT+DART simulations. *Remote Sens. Environ.* 127, 298–315.
- Jacquemoud, S., Baret, F., 1990. Prospect: a model of leaf optical properties spectra. *Remote Sens. Environ.* 34, 75–91.
- Jacquemoud, S., Ustin, S.L., Verdebout, J., Schmuck, G., Andreoli, G., Hosgood, B., 1996. Estimating leaf biochemistry using the PROSPECT leaf optical properties model. *Remote Sens. Environ.* 56, 194–202.
- Kroll, C., Stedinger, J., 1996. Estimation of moments and quantiles using censored data. *Water Resour. Res.* 32 (4), 1005–1012.
- Kuusik, A., 1985. The hotspot effect of a uniform vegetation cover. *Soviet J. Remote Sens.* 3, 646–658.
- le Maire, G., François, C., Dufrene, E., 2004. Towards universal broad leaf chlorophyll indices using PROSPECT simulated database and hyperspectral reflectance measurements. *Remote Sens. Environ.* 89, 1–28.
- Lillestaeter, O., 1982. Spectral reflectance of partly transmitting leaves: Laboratory measurements and mathematical modeling. *Remote Sens. Environ.* 12, 247–254.
- Martin, P., Zarco-Tejada, P., González, M.R., Berjon, A., 2007. Using hyperspectral remote sensing to map grape quality in 'tempranillo' vineyards affected by iron deficiency chlorosis. *Vitis* 46 (1).
- Meggio, F., Zarco-Tejada, P.J., Núñez, L.C., Sepulcre-Cantó, G., Gonzalez, M.R., Martin, P., 2010. Grape quality assessment in vineyards affected by iron deficiency chlorosis using narrow-band physiological remote sensing indices. *Remote Sens. Environ.* 114, 1968–1986.
- Merzlyak, M.N., Gitelson, A.A., Chivkunova, O.B., Rakitin, V.Y., 1999. Non destructive optical detection of leaf senescence and fruit ripening. *Physiol. Plant.* 106, 135–141.
- Miller, J.R., Steven, M.D., Demetriades-Shah, T.H., 1992. Reflection of layered bean leaves over different soil backgrounds: measured and simulated spectra. *Int. J. Remote Sens.* 13, 3273–3286.
- North, P.R.J., 1996. Three-dimensional forest light interaction model using a Monte Carlo method. *IEEE Trans. Geosci. Remote Sens.* 34 (4), 946–956.
- Peñuelas, J., Filella, I., Lloret, P., Muñoz, F., Vilajeliu, M., 1995. Reflectance assessment of mite effects on apple trees. *Int. J. Remote Sens.* 16 (14), 2727–2733.
- Riaño, D., Patricio, M.A., Zarco-Tejada, P.J., Rueda, C., Usero, L., Ustin, S.L., 2005. Estimation of equivalent water thickness using radial basis function neural networks. In: International Conference on Remote Sensing and Geoinformation Processing in the Assessment and Monitoring of Land Degradation and Desertification (RGLDD), Trier, Germany, 7–9, September 2005.
- Ritz, T., Damjanovic, A., Schulten, K., Zhang, J.P., Koyama, Y., 2000. Understanding efficient light-harvesting through carotenoids with novel theoretical and experimental techniques. *Photosynth. Res.* 66, 125–144.

- Rondeaux, G., Steven, M., Baret, F., 1996. Optimization of soil-adjusted vegetation indices. *Remote Sens. Environ.* 55, 95–107.
- Sims, D.A., Gamon, J.A., 2002. Relationships between leaf pigment content and spectral reflectance across a wide range of species, leaf structures and developmental stages. *Remote Sens. Environ.* 81, 337–354.
- Suárez, L., Zarco-Tejada, P.J., Sepulcre-Cantó, G., Pérez-Priego, O., Miller, J.R., Jiménez-Muñoz, J.C., Sobrino, J., 2008. Assessing canopy PRI for water stress detection with diurnal airborne imagery. *Remote Sens. Environ.* 112, 560–575.
- Suárez, L., Zarco-Tejada, P.J., González-Dugo, V., Berni, J.A.J., Sagardoy, R., Morales, F., Fereres, E., 2010. Detecting water stress effects on fruit quality in orchards with time-series PRI airborne imagery. *Remote Sens. Environ.* 114, 286–298.
- Thayer, S.S., Björkman, O., 1990. Leaf xanthophyll content and composition in sun and shade determined by HPLC. *Photosynth. Res.* 23, 331–343.
- Verhoef, W., 1984. Light scattering by leaf layers with application to canopy reflectance modeling: the SAIL model. *Remote Sens. Environ.* 16, 125–141.
- Wellburn, A.R., 1994. The spectral determination of chlorophylls a and b, as well as total carotenoids, using various solvents with spectrophotometers of different resolutions. *J. Plant Physiol.* 144, 307–313.
- Yamada, N., Fujimura, S., 1991. Nondestructive measurement of chlorophyll pigment content in plant leaves from three-color reflectance and transmittance. *Appl. Opt.* 30, 3964–3973.
- Young, A., Britton, G., 1990. Carotenoids and stress. In: Alscher, R.G., Cumming, J.R. (Eds.), *Stress Responses in Plants: Adaptation and Acclimation Mechanisms*, pp. 87–112.
- Zarco-Tejada, P.J., Miller, J.R., Mohammed, G.H., Noland, T.L., Sampson, P.H., 2001. Scaling-up and model inversion methods with narrow-band optical indices for chlorophyll content estimation in closed forest canopies with hyperspectral data. *IEEE Trans. Geosci. Remote Sens.* 39 (7), 1491–1507.
- Zarco-Tejada, P.J., Miller, J.R., Morales, A., Berjón, A., Agüera, J., 2004. Hyperspectral indices and model simulation for chlorophyll estimation in open-canopy tree crops. *Remote Sens. Environ.* 90 (4), 463–476.
- Zarco-Tejada, P.J., Berjón, A., López-Lozano, R., Miller, J.R., Martín, P., Cachorro, V., González, M.R., Frutos, A., 2005. Assessing vineyard condition with hyperspectral indices: leaf and canopy reflectance simulation in a row-structured discontinuous canopy. *Remote Sens. Environ.* 99, 271–287.
- Zarco-Tejada, P.J., Berni, J.A.J., Suárez, L., Fereres, E., 2008. A new era in remote sensing of crops with unmanned robots. *SPIE Newsroom*, <http://dx.doi.org/10.1117/2.1200812.1438>.
- Zarco-Tejada, P.J., Berni, J.A.J., Suárez, L., Sepulcre-Cantó, G., Morales, F., Miller, J.R., 2009. Imaging chlorophyll fluorescence from an airborne narrow-band multispectral camera for vegetation stress detection. *Remote Sens. Environ.* 113, 1262–1275.
- Zarco-Tejada, P.J., González-Dugo, V., Berni, J.A.J., 2012. Fluorescence, temperature and narrow-band indices acquired from a UAV platform for water stress detection using a micro-hyperspectral imager and a thermal camera. *Remote Sens. Environ.* 117, 322–337.